Delayed dynamics in an electronic relaxation oscillator

Angelo Di Garbo,[1] Stefano Euzzor,[2] Jean-Marc Ginoux,[3] F. Tito Arecchi,[2,4] and Riccardo Meucci[2,4]
[1]*CNR - Institute of Biophysics, Pisa, Italy*
[2]*CNR - National Institute of Optics, Florence, Italy*
[3]*CNRS, UMR 7020, Laboratory of Informatics and Systems, France*
[4]*Department of Physics and Astronomy, Universitá di Firenze, Firenze, Italy*

(Received 12 March 2019; published 27 September 2019)

We present an experimental investigation of the complex dynamics of a modulated relaxation oscillator implemented by using a unipolar junction transistor (UJT) showing the transition to chaos through torus breakdown. In a previous paper a continuous model was introduced for the same system, explaining chaos based on analogy with a memristor. We propose here a new approach based on a piecewise linear model with delay considering a measured parasitic delay effect. The inclusion of this delay, accounting for memory effects, increases the dimensionality of the model, allowing the transition to chaos as observed in the experiment. The piecewise delayed model shows analogies with a two-dimensional leaky integrate-and-fire model used in neurodynamics.

DOI: 10.1103/PhysRevE.100.032224

I. INTRODUCTION

Relaxation oscillators constitute a large class of nonlinear oscillators distinct from linear oscillators. In electronic implementations a linear oscillator makes use of a transistor or an operational amplifier; the key tool to obtain oscillation is a feedback loop, whereby the intrinsic noise is amplified and returned to the input, yielding a stable sinusoidal output. In contrast, relaxation oscillators are nonlinear and their output shape is nonsinusoidal [1,2]. A relaxation oscillator consists of an energy-storing element such as a capacitor and a nonlinear switching device such a Schmitt trigger comparator or *negative resistance* element connected by a feedback loop. The switching device periodically charges and discharges the energy stored in the capacitor, yielding abrupt changes in the output waveform. The concept of "relaxation oscillation" was introduced by Balthasar van der Pol to distinguish from linear oscillators [3] and to characterize the solutions of *slow-fast* dynamical systems (see also work by Ginoux [4,5]).

Recently the van der Pol experiment on a glow discharge neon tube was revisited [6]. The experiments display the quasiperiodic route to chaos, with the two competing frequencies being the relaxation frequency and the plasma eigenfrequency. Based on the volt-ampere characteristic of the discharge, a macroscopic model of the current flowing in the plasma has been proposed. The model, governed by four autonomous ordinary differential equations, is used to compute stability diagrams for periodic oscillations of arbitrary period in the control parameter space of the discharge. In order to have a better separation between the roles played by the relaxation frequency imposed by the *RC* components and the intrinsic plasma oscillation, a relaxation oscillator based on a unipolar junction transistor (UJT) [1,2] has been implemented. This device possesses a *negative resistance* and its current-voltage characteristic can be fitted with that of a memristor [7–9]. When the UJT oscillator is coupled in a bidirectional way with a harmonic oscillator, it displays quasiperiodic behavior and torus breakdown. Evidence of chaos has been reproduced by a continuous four-dimensional model based on the memristor analogy [10]. The derivation of the model, following the same strategy adopted for a low pressure discharge tube, includes the effects of a parasitic inductance, which is justified for a discharge but artificially used for the UJT oscillator. Furthermore, the transition to chaos in the model is not the same as the observed one. Indeed, the model foresees the following transition to chaos as the control parameter is increased: limit cycle ($m = 0$), abrupt transition to chaos ($0 < m < 0.5$), followed by a torus region ($0.5 < m < 1$).

The aim of this work is to adopt a different approach to the dynamics of the UJT oscillator. More precisely, the experimental observations of the spiking signals indicate that a piecewise model distinguishing the *slow* charge from the *fast* processes seems more appropriate. With proper threshold conditions on the voltage signal on the capacitor C and resetting conditions for the successive cycle, several of the experimental results can be explained by including quasiperiodic (torus attractors) and periodic behavior (phase locking regimes); however, torus breakdown leading to chaos remains to be explained. The experimental evidence of a small parasitic delay in the UJT signals justifies the introduction of delay terms in the piecewise model, becoming the key feature to give rise to chaos. The adopted model shows analogies with the integrate-and-fire dynamics used as a simple approach to neuron spiking activity. Single-cell spiking oscillators are of the relaxation type, characterized by a *slow* charging phase, threshold condition, and generation of a *fast* action potential [11]. Most biological oscillators are of the *relaxation type*, sometimes also named pulsatile oscillators. These oscillators are largely used to describe many phenomena in biology [12], chemistry [13,14], and electronics [1,2]. Recently, evidence of chaotic dynamics was reported in relaxation oscillators using

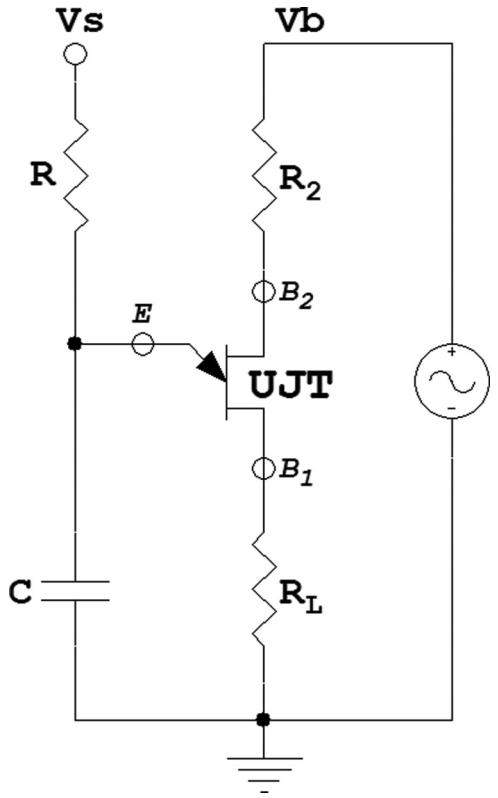

FIG. 1. Representation of the UJT circuit employed in the experiment.

NbO_2 Mott memristors [15]. In such nanoscale devices, chaos emerges due to the nonlinear current transport coupled with thermal fluctuations.

The paper is organized as follows. After this introduction, a short description of the experiment is presented, focusing on the Poincaré section as the key indicator. Sec. III contains a detailed derivation of the piecewise model and the introduction of a delayed term. In Sec. IV, the simulations are presented and compared with the experimental results. Two subsections, one on phase dynamics and the other on torus breakdown, are included. In the latter one the role of delay emerges as the crucial one to yield the transition to chaos. In the concluding section, the analogies with a neural model are discussed.

II. EXPERIMENT DESCRIPTION

Here we provide a short description of the experimental setup. A schematic representation of a driven UJT relaxation oscillator is reported in Fig. 1. The UJT is a Motorola 2N2646 and it is connected from the emitter side E through the resistor R (12.7 kΩ) to the supply voltage V_s fixed at 7.0 V. On the B2 base, it is connected to a modulated bias voltage where the constant value is fixed at $V_b = 4.8$ V. The resistor R_L (56 Ω) is a load resistor on which the discharge current through the UJT is detected as a voltage signal. The capacitor C has a value of 49.7 nF.

The typical temporal behavior of this oscillator at a frequency of 4470 Hz is shown in Fig. 2. The top panel shows the two main stages of the UJT dynamics. The first one is

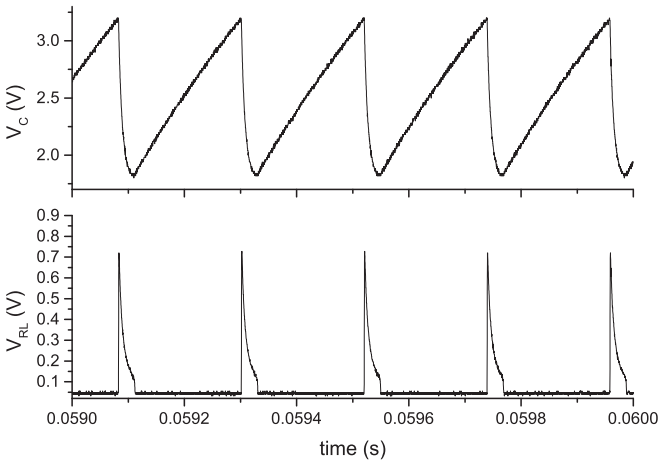

FIG. 2. In the top (bottom) panel we plotted the time evolution of the potential across the capacitor (the resistor R_L) during the charging (discharging) phase in the absence of periodic modulation.

characterized by a *slow* charging process of the capacitor C with a *relaxation time* constant RC; the second one is a *fast* discharging process through the UJT. The fast process starts immediately after a given voltage threshold is reached. A reduction of V_s implies an increase of the oscillation frequency up to the point where the UJT oscillator stops working (about 9000 Hz when V_s is close to 2.5 V).

In a previous work [10] it was stated that the characteristic of oscillations of the UJT can be modeled by a nonlinear mathematical function having a *falling branch*. Thus, even in the absence of the external modulation this system is capable of generating stable *self-sustained oscillations* [4,5].

The dynamics of the UJT relaxation oscillator was tracked in real time by Poincaré sections implemented on the current signal on the load resistor R_L. The apparatus for recording the Poincaré's sections (not shown in Fig. 2) included sample-and-hold circuits to memorize the peaks of the current signal I_n as well as the same sequence delayed by one peak, I_{n-1}. The two sequences were plotted in x-y configuration on a digital oscilloscope (Tektronix TDS7104).

III. MODEL DESCRIPTION

The dynamical behavior reported in Fig. 2 shows a *slow* accrual charge phase and a *fast* discharge phase. Based on it, we build a mathematical model for the UJT *relaxation oscillator*. Following this analogy, the schematic circuit reported in Fig. 3(a) will be used to describe the two working phases of the UJT circuit: charging and discharging of the capacitor C. During the charging process the position of the switch is that reported in Fig. 3(a), and the resistor R_{b1} assumes its higher value ($R_{b1\,\mathrm{high}}$). When the potential across the capacitor reaches the threshold value the switch is instantaneously moved to the right position, allowing a *fast* discharge. During this phase, the value of the resistance R_{b1} assumes its lower value ($R_{b1\,\mathrm{low}}$). Figure 3(b) shows the static electric characteristic V_E-I_E of the used UJT together with its negative resistance R_{b1} (in the model R_{b1} will be assumed to switch between $R_{b1\,\mathrm{high}} = 2400$ Ω and $R_{b1\,\mathrm{low}} = 180$ Ω).

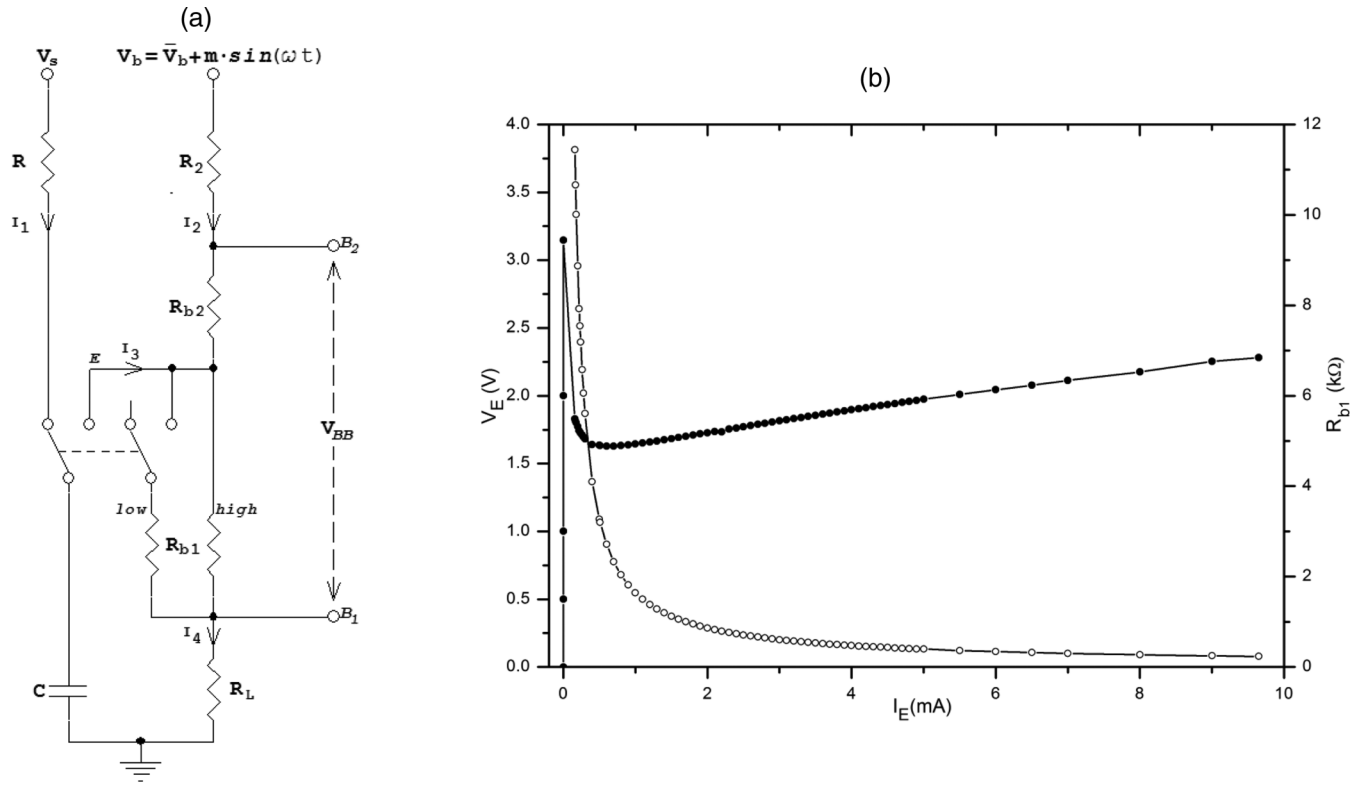

FIG. 3. (a) Schematic representation of the circuit. The UJT has been replaced by a switch (double-pole two-way switch) allowing separation between the charging of the capacitor C and its discharge through the series resistors $R_{b1\,\mathrm{low}} + R_L$. (b) Static electric characteristic V_E-I_E (filled circles) and R_{b1} versus I_E (empty circles).

Assignment of the threshold value and resetting condition completes the UJT model. With reference to Fig. 3(a), let $I_1 = \frac{dq}{dt}$ be the current flowing through the resistance R, I_2 the current flowing in the resistances R_2 and R_{b2}, I_3 the emitter current, and $I_4 = I_2 + I_3$. Then, by Kirchhoff's laws, the equations describing the subthreshold dynamics of the UJT model (tUJT) are, for the charging phase,

$$V_s = R\frac{dq}{dt} + \frac{q}{C} \tag{1}$$

and, for the discharging phase,

$$V_b(t) = (R_2 + R_{b2})I_2 + R_{b1\,\mathrm{low}}I_4, \tag{2}$$

$$I_4 = I_2 + I_3, \tag{3}$$

$$\frac{q_1}{C} = (R_{b1\,\mathrm{low}} + R_L)I_4. \tag{4}$$

In the above equations $V_b(t) = V_{b0} + m\sin(\omega t)$ is a modulated bias potential. In addition, $I_3 = -\frac{dq_1}{dt}$. where q_1 is the charge on the capacitor during the discharge phase. From Eqs. (3) and (4) it follows that $I_4 = q_1/C(R_{b1\,\mathrm{low}} + R_L)$ and $I_2 = I_4 - I_3$. Then Eqs. (1)–(4) reduce to the following system:

$$\frac{dq}{dt} = \frac{V_s}{R} - \frac{q}{RC}, \tag{5}$$

$$\frac{dq_1}{dt} = \frac{V_b(t)}{R_2 + R_{b2}} - \frac{R_A q_1}{C(R_{b1\,\mathrm{low}} + R_L)(R_2 + R_{b2})}, \tag{6}$$

where $R_A = R_2 + R_{b2} + R_{b1\,\mathrm{low}} + R_L$. It is convenient to introduce an adimensional time $t' = t/RC$. Then, by setting $\bar{q}(t') = q(RCt')$, $\bar{q}_1(t') = q_1(RCt')$, $\bar{V}_b(t') = V_b(RCt')$, the previous system of differential equations reads

$$\frac{d\bar{q}}{dt'} = V_s C - \bar{q}, \tag{7}$$

$$\frac{d\bar{q}_1}{dt'} = \frac{RC}{R_2 + R_{b2}}\bar{V}_b(t') - \bar{q}_1\frac{RR_A}{(R_{b1\,\mathrm{low}} + R_L)(R_2 + R_{b2})}. \tag{8}$$

This linear system describes the subthreshold dynamics of the tUJT and possesses a stable stationary state. Thus, starting from any initial condition, all trajectories, after a suitable transient, decay to the stable state. In order to generate the spiking dynamics, we need to modify the tUJT model by introducing some *ad hoc* mechanisms. In particular, in analogy with some models in neurophysiology, the tUJT model is modified by introducing a threshold value, $\bar{q}_T$. When $\bar{q}(t')$ reaches $\bar{q}_T$ the values of $\bar{q}$ and $\bar{q}_1$ are reset to $\bar{q}_R$ and $\bar{q}_{1R}$ respectively. After that, the solutions of Eqs. (7) and (8) restart from the initial conditions $\bar{q}(t_n) = \bar{q}_R$, $\bar{q}_1(t_n) = \bar{q}_{1R}$, where t_n is the threshold crossing time. In this way, the tUJT model is capable of generating periodic (and also more complex) oscillatory dynamics. With these assumptions the dynamical system describing the tUJT becomes lumpy (no longer smooth) and nonlinear (both properties arise from the resetting). The experimental data reported in Fig. 2 suggest the resetting condition, by evaluation of the potential at the end of the discharge phase of the capacitor as a fraction of that reached at threshold. Thus, in the model we assume that $\bar{q}_R = \alpha\bar{q}(t'_n)$, where $0 < \alpha < 1$. Instead, the resetting condition for $q_1(t')$ is assumed to be $\bar{q}_{1R} = \bar{q}(t'_n) + \bar{q}_1(t'_n)$, where $\bar{q}(t_n)$ and $\bar{q}_1(t_n)$ are the values of these charges at threshold.

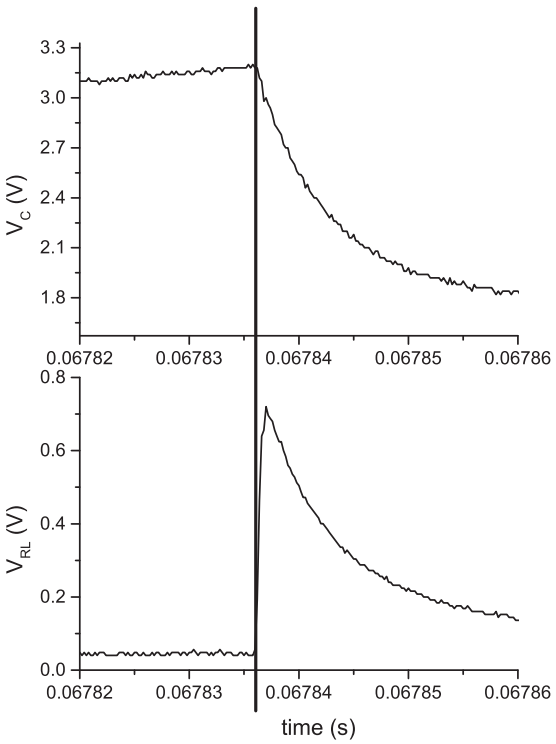

FIG. 4. Top panel shows the voltage across the capacitor C during the charging phase in absence of periodic modulation. Bottom panel shows the voltage peak read through resistor R_L occurring with a delay $\tau = 1\ \mu$s.

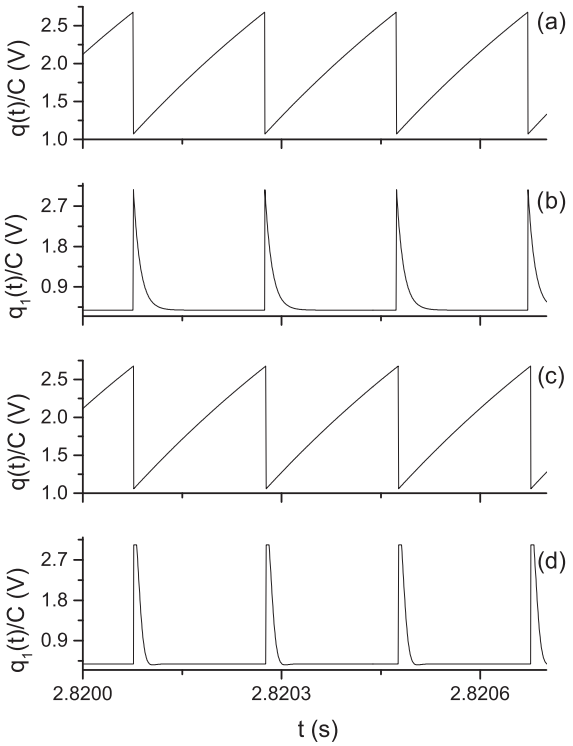

FIG. 5. Results from the tUJT model in the absence of periodic stimulation. (a) The time evolution of the potential across the capacitor during the charging phase; (b) corresponding time evolution of the potential q_1/C during the discharging phase of the capacitor in the case $\tau = 0\ \mu$s. (a) and (d) Results for $\tau = 0.5\ \mu$s.

According to the literature on UJTs [16], the threshold voltage is given by $V_T = V_0 + \eta \bar{V}_{\rm BB}$, where $V_0 = 0.7V$ and $\eta = R_{b1\,\rm high}/(R_{b2} + R_{b1\,\rm high})$. Using realistic values for these two resistors ($R_{b2} = 2100\ \Omega$ and $R_{b1\,\rm high} = 2400\ \Omega$) leads to a value of η which is in the UJT expected range. Using Eq. (8) and the tUJT circuit representation of Fig. 3, one can write the potential $\bar{V}_{\rm BB}$ as follows: $\bar{V}_{\rm BB}(t') = p_1 \bar{q}_1(t') + p_2 \bar{V}_b(t')$, where $p_1 = (R_2 R_{b1\,\rm low} - R_{b2} R_L)/[C(R_{b1\,\rm low} + R_2)(R_2 + R_{b2})]$ and $p_2 = R_{b2}/(r_2 + R_{b2})$. Then, using this last equation, the threshold for $\bar{q}(t')$ is well defined as $\bar{q}_T = C[V_0 + \eta \bar{V}_{\rm BB}(t')]$. It is worthwhile to point out that $\bar{V}_{\rm BB}(t')$ also includes the contribution of the discharge phase through $\bar{q}_1$, thus an indirect coupling with the charging phase is present. Finally, by setting $x(t') = \bar{q}(t')/(V_S C)$ and $y(t') = \bar{q}_1(t')$, Eqs. (7) and (8) become

$$\frac{dx}{dt'} = 1 - x(t') \tag{9}$$

$$\frac{dy}{dt'} = \frac{RC}{R_2 + R_{b2}} \bar{V}_b(t') - y(t') \frac{RR_A}{(R_{b1\,\rm low} + R_L)(R_2 + R_{b2})}, \tag{10}$$

where the threshold value for $x(t')$ is given by $x_T = \bar{q}_T/(V_S C) = (V_0 + \eta \bar{V}_{\rm BB})/V_S$. When the variable $x(t')$ crosses the threshold (at time t_n), the following resetting conditions are employed: $x_R = \alpha x(t_n)$ and $y_R = y(t_n) + V_S C x(t_n)$, where $x(t_n)$ and $y(t_n)$ are the values of $x(t')$ and $y(t')$ at threshold, and this implies the coupling between the two variables. In this way the tUJT model, described by the previous system of equations, is similar to a two-dimensional integrate-and-fire neuronal model [17–19]. According to Ref. [19] we can compare our x variable with a membrane voltage v and our y variable with a dynamic threshold s. As explained later, the tUJT model is not capable of reproducing the occurrence of torus breakdown, although it is nonlinear. In order to reproduce this feature we need to increase the dimensionality of our model. Since the experimental data on the UJT circuit reveal that there is a parasitic delay between the peak of the discharge current and the potential across the capacitor (see Fig. 4), the introduction of a delay dynamics is justified. This effect is in agreement with the investigations on semiconductor-ferromagnet junctions in the spin-blockade regime by Pershin and Di Ventra [20] and in a neuron based electronic switch by James *et al.* [21]. The role of a short delay in providing additional degrees of freedom necessary to observe the transition to chaos has been addressed in laser dynamics by Arecchi *et al.* [22]. Since it has been established in a previous work that the UJT behaves like a memristor [10], such a delay corresponds to the memory of the previous state, i.e., the "persistence of memory." Parasitic effects in memristor devices have been studied by Jeong *et al.* [23] using a piecewise linear function. The tUJT model is modified by introducing a delay τ in Eq. (10), and the delayed model is rewritten as follows:

$$\frac{dx}{dt'} = 1 - x(t'), \tag{11}$$

$$\frac{dy}{dt'} = \frac{RC}{R_2 + R_{b2}} \bar{V}_b(t') - y(t' - \tau) \frac{RR_A}{(R_{b1\,\rm low} + R_L)(R_2 + R_{b2})} \tag{12}$$

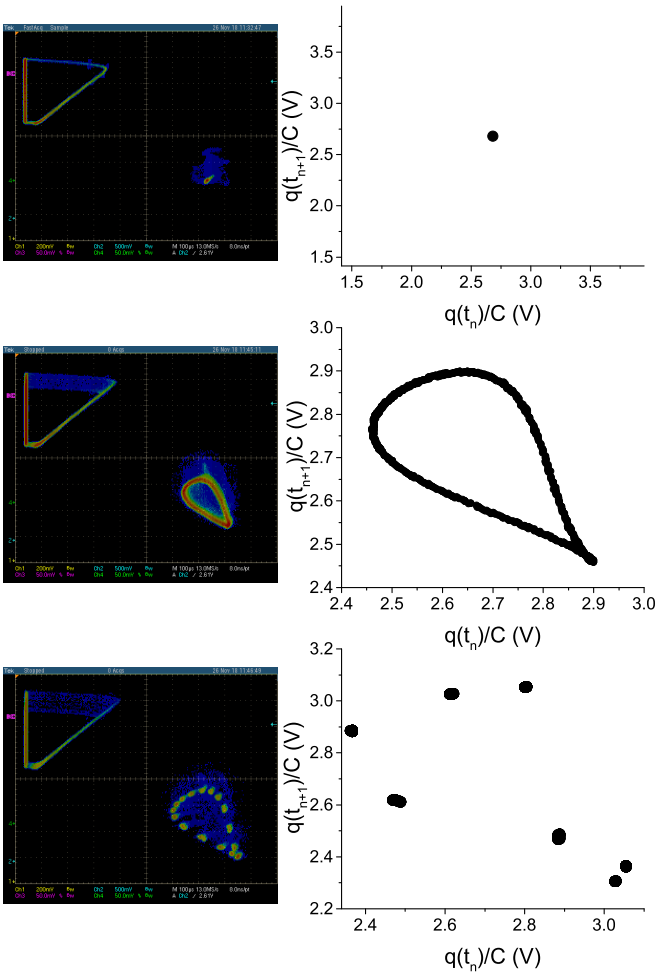

FIG. 6. First return maps of experimental and theoretical results where the modulation frequency is equal to the golden mean. Inside the left panels we plotted both the first return map (bottom right of each panel) and the attractor (top left of each panel) of the experimental data for increasing values (for $m = 0$ V, $m = 0.232$ V, $m = 0.336$ V from top to bottom) of the amplitude of the modulation. In the right ones we show the corresponding return maps for the tUJT (for $m = 0$ V, $m = 0.541$ V, $m = 0.940$ V from top to bottom). The theoretical data were obtained for $\tau = 0.5$ μs.

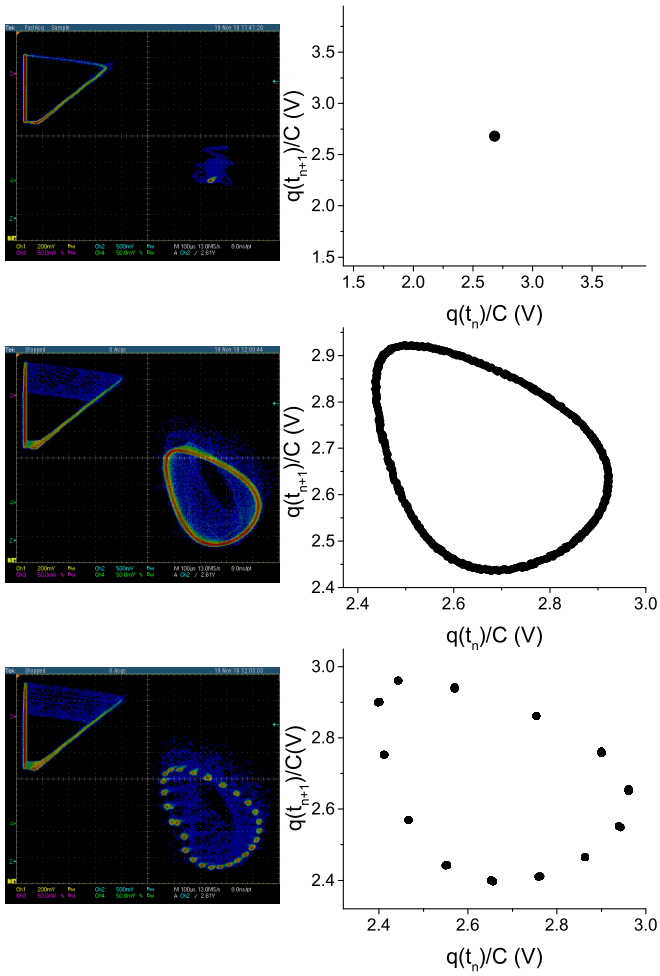

FIG. 7. First return maps of experimental and theoretical results where the modulation frequency is equal to the half of the golden mean. Inside the left panels we plotted both the first return map (bottom right of each panel) and the attractor (top left of each panel) of the experimental data for increasing values (for $m = 0$ V, $m = 0.490$ V, $m = 0.510$ V from top to bottom) of the amplitude of the modulation. In the right ones we show the corresponding return maps for the tUJT (for $m = 0$ V, $m = 0.600$ V, $m = 0.700$ V from top to bottom). The theoretical data were obtained for $\tau = 0.5$ μs.

with delayed resetting conditions $x_R = \alpha x(t_n - \tau)$ and $y_R = y(t_n - \tau) + V_S C x(t_n - \tau)$. On the basis of the experimental data the value of such delay is $\tau = 0.5$ μs. In the next sections we will show that, with such a choice, the tUJT model is able to reproduce the experimental features.

IV. NUMERICAL RESULTS

A. Dynamical behavior of the model in the absence of periodic modulation

Let us start by considering Eqs. (11) and (12), where the bias potential is a constant ($V_b(t) = V_{b0} = 4.9V$). In the experiment the free oscillation frequency of the UJT circuit is approximatively 5000 Hz while the oscillation period in the tUJT model depends on the value of the parameter α used in the resetting of $x(t')$. Therefore, to fit the experimental data, the value of α is set to 0.4. With this choice, and $\tau = 0.5$ μs, the free oscillation frequency of the tUJT is $\nu_{\text{free}} \simeq 5003$ Hz.

In Fig. 5(a) we plotted the time evolution of the potential $q(t)/C$ across the capacitor in the absence of delay. The time evolution of the potential $q_1(t)/C$, characterizing the discharge phase through the resistor R_L, is plotted in Fig. 5(b). For the sake of completeness Figs. 5(c) and 5(d) show the delayed case for $\tau = 0.5$ μs.

B. Periodic stimulation of the UJT oscillator

Let us now introduce a time modulation of the bias potential: $V_b(t) = V_{b0} + m\sin(\omega t)$, where $\omega = 4\pi\nu_{\text{free}}/(1+\sqrt{5})$ (golden mean frequency). A powerful approach to analyze the experimental and theoretical results is to use a discrete two-dimensional representation of the dynamics. In our case this is achieved by plotting the following set of points:

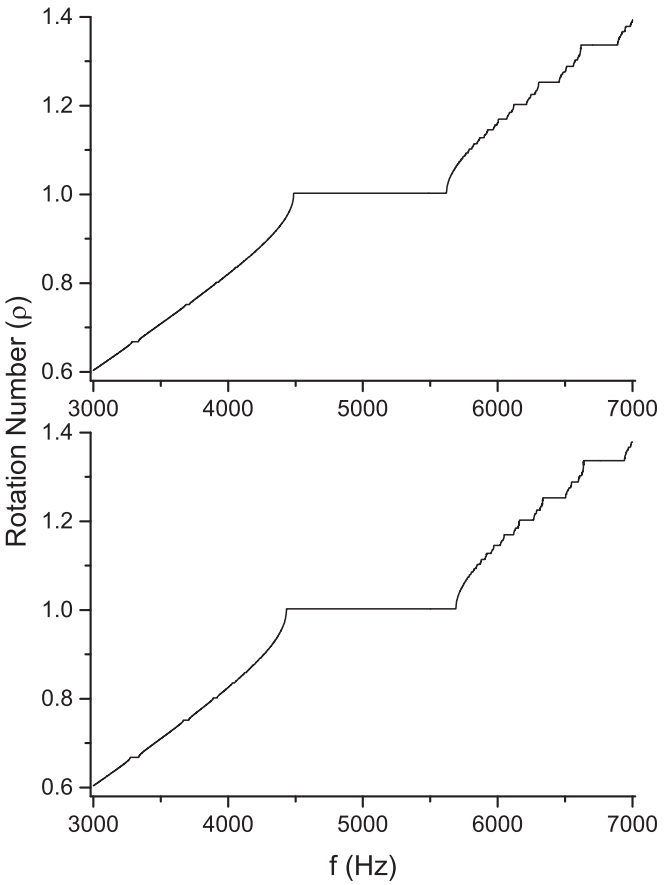

FIG. 8. Dependence of the rotation number on the modulation frequency (f). The data in the top panel refer to the parameter values corresponding to the torus for the golden mean frequency case ($m = 0.541$ V), while those in the bottom panel correspond to half the golden mean case ($m = 0.600$ V). For both panels $\tau = 0.5$ μs.

$Q = \{(q(t_n)/C, q(t_{n-1})/C,\ n = 1, 2, \dots\}$, where $q(t_n)$ represents the value of the capacitor charge when the threshold is crossed (at time t_n). Thus, the set Q is the first return map or Poincaré section of the system. In the left panels of Fig. 6 we report the experimental data for different values of the modulation amplitude (m). At $m = 0$ V the circuit exhibits periodic oscillation which is $q(t_n)/C = q(t_{n-1})/C]$ and, as expected, the corresponding set Q reduces to a point (left top panel). When m is increased, a transition towards a quasiperiodic dynamical regime (torus) is observed (left middle panel). Further increasing the modulation amplitude (left bottom panel) leads to the appearance of periodic oscillations (phase locking motion). The right panels report the corresponding results for the tUJT model and for $\tau = 0.5$ μs. The data in the top right panel are obtained for $m = 0$ V and show a period-1 oscillation; the data in the right middle panel show the occurrence of a quasiperiodic orbit (torus) for $m = 0.541$ V that becomes a periodic one when $m = 0.94$ V (bottom right panel).

In Fig. 7 we report the corresponding results when the ratio between the frequencies is reduced to half the golden mean. The comparison between experimental and theoretical results shows that the tUJT model mimics very well the experimental data in this case as well.

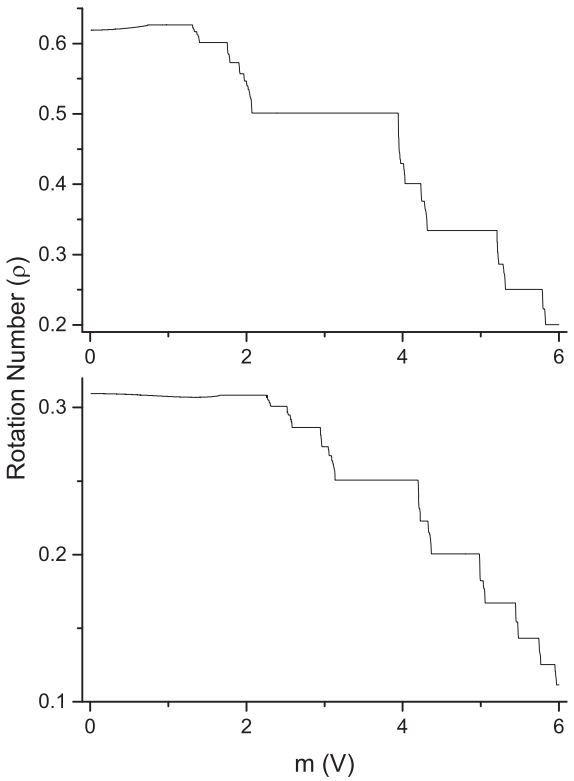

FIG. 9. Dependence of the rotation number on the amplitude of the modulation (m). The data in the top panel refer to the parameter values corresponding to the torus for the golden mean frequency case [$\omega = \omega_{\rm GM} = 4\pi\nu_{\rm free}/(1+\sqrt{5})$], while those in the bottom panel correspond to half the golden mean case ($\omega = \omega_{\rm GM}/2$). For both panels $\tau = 0.5$ μs.

C. Phase properties of the UJT model

A different approach to the dynamics of a complex system subject to an external periodic forcing is that of introducing a suitable definition of its phase and tracking its time evolution [24]. We introduce this concept in a general setting and then apply this tool to investigate the tUJT dynamics. Let us consider, for instance, a continuous time dynamical system perturbed by an external periodic forcing of period T. Let $\mathbf{z}(t) \in \mathbb{R}^m$ be the corresponding state and $S = \{t_i \mid F(\mathbf{z}(t_i), t_i) = 0\}$ a sequence of times, where F is an assigned function. In other words, if t_i is such that $F(\mathbf{z}(t_i), t_i) = 0$, then $t_i \in S$. Let us assume that the set S is not empty and contains infinite elements with $t_i < t_{i+1}$, i.e., the sequence of t_i increases monotonically. Using the above definition we are now able to define the phase of the dynamical system for each $t_i \in S$, and such information can be employed to investigate the dynamical behavior of the system in a simpler way. More precisely, the phase of the dynamical system at t_i is defined as $\phi_i = \frac{t_i}{T} (\mathrm{mod}\ T)$, with $\phi_i \in [0, 1]$. In addition let us assume that $\forall i \in \mathbb{N}$ it is $\phi_{i+1} = G(\phi_i)$, where G is a circle map expressing the functional relationship between two consecutive phases. The lift of the map G is defined by $\phi^*_{i+1} = \bar{G}(\phi^*_i)$, with $\phi^*_i = \frac{t_i}{T} \in \mathbb{R}^+$ and $\bar{G} : \mathbb{R} \longrightarrow \mathbb{R}$. Then, the rotation number of the circle map G is defined as $\rho = \lim_{i\to\infty} (\frac{\phi^*_i}{i})$, when such a limit exists. Using the definition of the phase, the above expression can also be expressed as $\rho = \lim_{i\to\infty} (\frac{t_i}{iT})$.

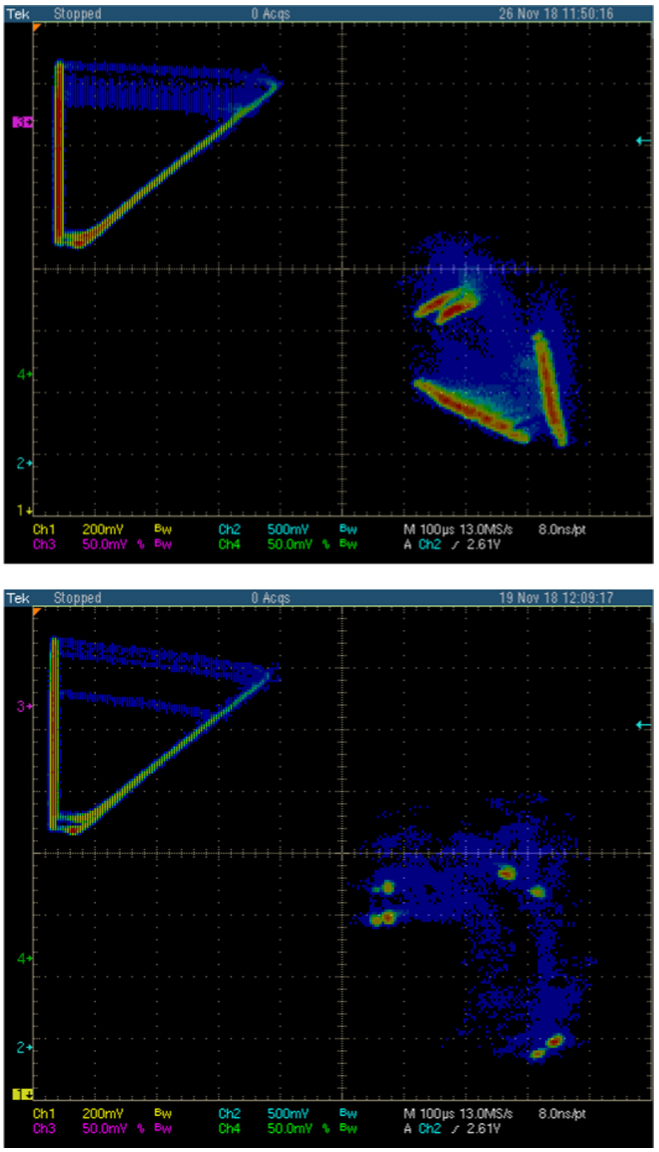

FIG. 10. Experimental data showing torus breakdown for a modulation frequency equal to the golden mean (top panel, $m = 0.394$ V) and for a modulation frequency equal to the half of the golden mean (bottom panel, $m = 0.530$ V). Inside each panel the first return map is shown in the bottom right and the attractor is shown in the top left side.

Now we study the dynamics of the tUJT by applying the above theory to our problem. In this case the set $S = \{t_i \mid F(\mathbf{z}(t_i), t_i) = 0\}$ contains the sequence of times $(t_i,\ i = 1, 2, \dots)$ defined by the condition $F(x(t_i), y(t_i), t_i) = x(t_i) - x_T(t_i) = 0$, where x_T is the threshold of the tUJT model defined previously. The estimation of ρ is performed by evaluating the ratio $\phi_i/(iT)$ for a large value of i. In the top panel of Fig. 8, we plot the values of ρ against the modulation frequency ν for a fixed value of the modulation amplitude ($m = 0.541$ V). Phase locking patterns occur for several values of ν and the larger interval is approximatively centered at $\nu = \nu_{\text{free}}$ (as expected). Similar results occur also for half the golden mean case with $m = 0.6$ V (bottom panel). Then, similar simulations are performed to study the dependence of the rotation number on the modulation amplitude m for a fixed modulation frequency. The data for the golden mean case $[\omega = \omega_{\text{GM}} = 4\pi\nu_{\text{free}}/(1+\sqrt{5})]$ are reported in the top panel of Fig. 9. The data show that several phase

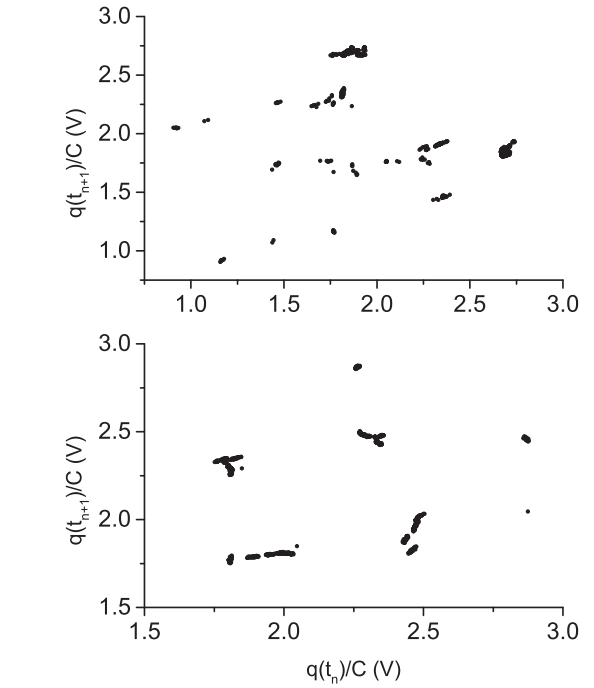

FIG. 11. First return maps obtained with the tUJT showing torus breakdown using 240 000 points. Top panel: data where the modulation frequency is equal to the golden mean and $\tau = 2$ μs, $m = 1.620$ V. In the bottom panel we show the the data when the modulation frequency is equal to half the golden mean and $\tau = 2$ μs, $m = 1.100$ V.

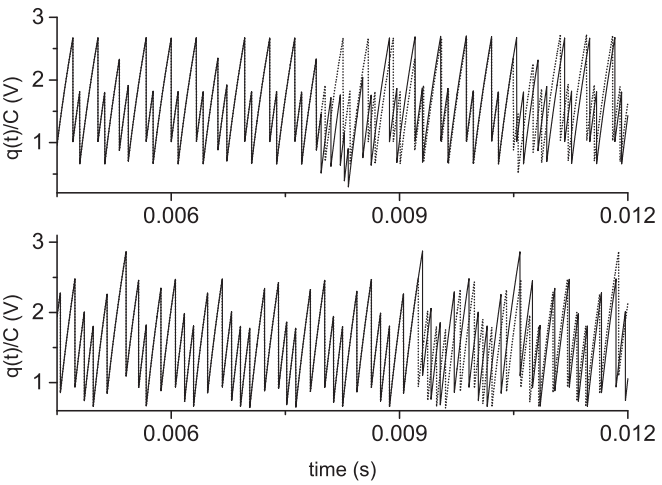

FIG. 12. Sensitivity to the initial conditions. For both panels the initial conditions are the following: solid line, $q(0)/C = 0.331 \times 10^{-13}$ V, $q_1(0)/C = 1.0 \times 10^{-13}$ V; dashed line, $q(0)/C = 0.192 \times 10^{-9}$ V, $q_1(0)/C = 1.0 \times 10^{-13}$ V. Top panel: data when the modulation frequency is equal to the golden mean and $m = 1.620$ V; the maximum Lyapunov exponent is $\lambda_{\text{max}} = 0.0963 \pm 0.0009$. Bottom panel: data when the modulation frequency is equal to half the golden mean and $m = 1.100$ V; the maximum Lyapunov exponent is $\lambda_{\text{max}} = 0.0851 \pm 0.0007$. For both panels $\tau = 2$ μs.

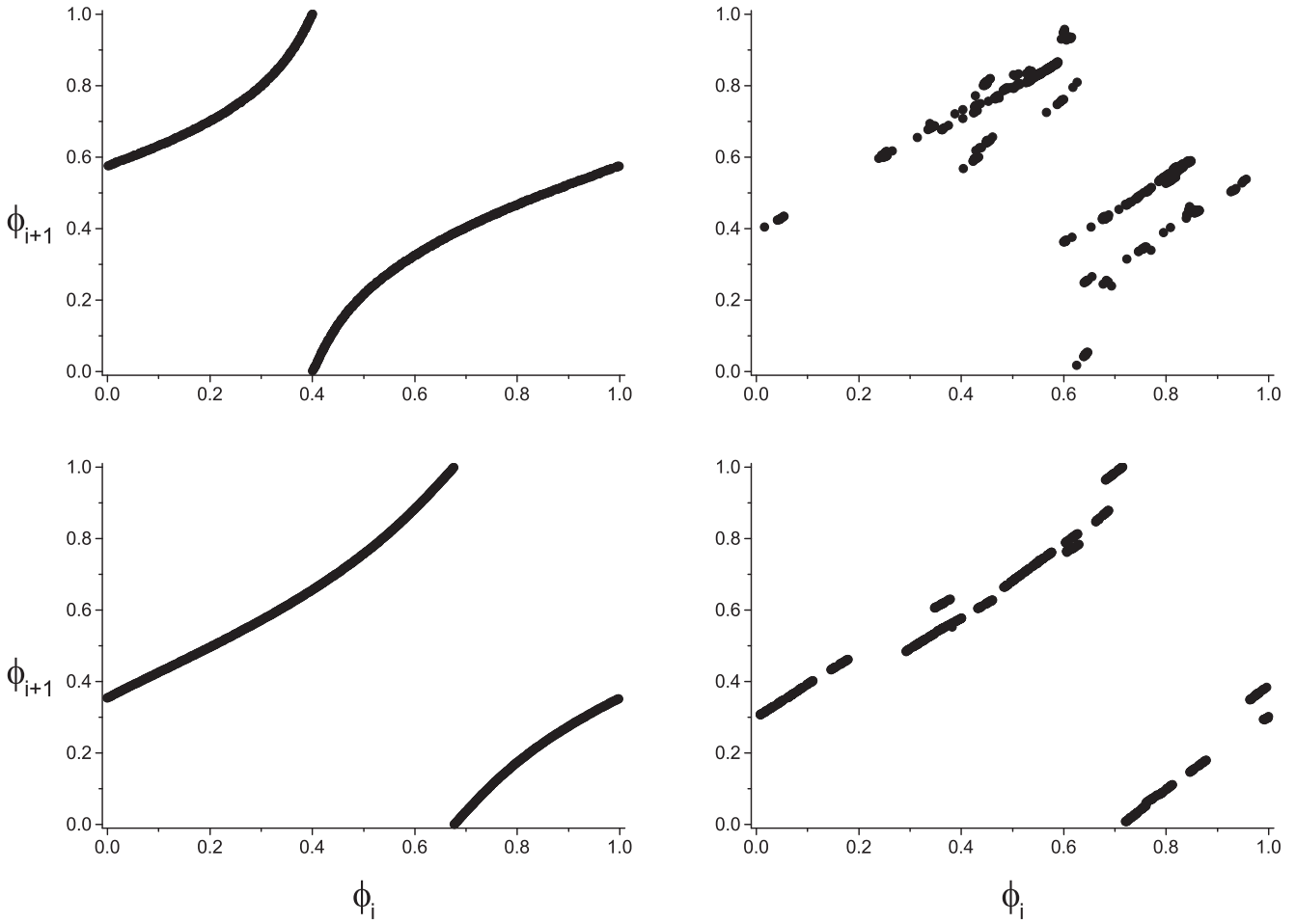

FIG. 13. Properties of the phase maps in the case of quasiperiodic dynamics and torus breakdown. Top panel: data corresponding to a modulation frequency equal to the golden mean. Left top panel: $\tau = 0.5$ μs, $m = 0.541$ V; right top panel $\tau = 2$ μs, $m = 1.620$ V. Bottom panel: data when the modulation frequency is half the golden mean. Left bottom panel: $\tau = 0.5$ μs, $m = 0.600$ V; right bottom panel $\tau = 2$ μs, $m = 1.100$ V.

locking patterns occur, and the largest one falls within the interval [2, 4] V. Similar results are obtained for a modulation frequency $\omega_{GM}/2$, and the corresponding data are reported in the bottom panel.

D. Torus breakdown and chaotic dynamics in the UJT circuit

Let us now consider torus breakdown as the parameter m is increased beyond after the locking regimes. This route to chaos in electronic circuits was explored by Matsumoto *et al.* [25] and Baptista and Caldas [26]. In the top panel of Fig. 10, we report torus breakdown when the modulation frequency is set to the golden mean ratio. Similar results were found also for half the golden mean ratio (bottom panel of Fig. 10). Starting from these experimental results, several simulations of the tUJT model were performed, aiming to get a similar dynamical behavior. The model with $\tau = 0.5$ μs does not reproduce torus breakdown but only periodic (or quasiperiodic) dynamics with a decreasing number of spots on the Poincaré section, as observed in the experiment. An accurate tuning of the delay τ is needed to get torus breakdown. In Fig. 11, evidence of torus breakdown is reported for $\tau = 2$ μs and $m = 1.62$ V. It is important to note that the tuning of this value occurs on fast timescale dynamics.

Similarly, at half the golden mean ratio, torus breakdown occurs for the same τ value and $m = 1.1$ V (bottom panel of Fig. 11). In both cases the tUJT model at the torus breakdown exhibits sensitivity to the initial conditions, as shown in Fig. 12 [27,28]. In addition, a quantitative measure of this complex dynamical behavior is achieved by estimating the corresponding maximum Lyapunov exponents for both cases reported in Fig. 12. To this aim we generated time series, each containing the values of the capacitor potential at the threshold, and then the corresponding maximum Lyapunov exponent was estimated by adopting the method proposed in Ref. [29]. To have statistically significant results, $n_r = 10$ time series were generated by using random initial conditions, and then for each of them the corresponding maximum Lyapunov exponent $[\lambda_{\max}(j), \quad j = 1, 2, \ldots, n_r]$ was estimated. Then, for each modulation regime, the corresponding mean value of the maximum Lyapunov exponent was computed as $\lambda_{\max} = [\sum_{j=1}^{n_r} \lambda_{\max}(j)]/n_r$, and the error of the mean as $\sigma/\sqrt{n_r}$. For the data reported in the top panel of Fig. 12 the maximum Lyapunov exponent is $\lambda_{\max} = 0.0963 \pm 0.0009$,

while for those in the bottom panel $\lambda_{\max} = 0.0851 \pm 0.0007$. To get more insight into these chaotic regimes, the corresponding phase maps are computed and compared with the quasiperiodic dynamics. The upper panels of Fig. 13 correspond to the golden mean ratio, while the lower ones correspond to half the golden mean ratio. Clearly the maps on the left side are invertible while those on the right are not. Similarly, in the left bottom panel we show the results for the case at half of golden mean modulation frequency ($\tau = 2\ \mu$s, $m = 0.6$ V). Also in this case the map is invertible. The right panels give the results when a torus breakdown occurs and the corresponding maps are no longer invertible. In conclusion, the experimental data on torus breakdown, the loss of invertibility of the map, and the sensitivity to the initial conditions suggest that some dynamical regimes of the tUJT are compatible with chaotic dynamics.

V. CONCLUSION

In this work we have reported experimental evidence of torus breakdown in a driven UJT oscillator. The results have been explained by using a nonsmooth delayed dynamical system where the delay time plays a crucial role in the transition to chaos, requiring an accurate tuning. The presence of delay effects remains consistent with the fact that the UJT can be considered as a memristor, that is, a nonlinear resistor with memory, as recently studied by using a continuous four-dimensional model [10], with the advantages of providing the correct sequence to chaos as in the experiment and possessing a strict analogy with neurodynamics. The results are in agreement with those obtained by Chacron *et al.* [19], where chaos in a modulated LIF model is obtained only when memory effects are strong and the threshold includes nonlinear fatigue functions.

[1] J. Millmann and H. Taub, *Pulse, Digital and Switching Waveforms* (McGraw-Hill, New York, 1965), p. 972.

[2] P. Horowitz and W. Hill, *The Art of Electronics* (Cambridge University Press, Cambridge, 2015), p. 428.

[3] B. van der Pol, On "relaxation-oscillations", London Edinburgh Dublin Philos. Mag. J. Sci. (VII) **2**, 978 (1926).

[4] J.-M. Ginoux, *History of Nonlinear Oscillation Theory in France (1880–1940)*, Archimedes Series Vol. 49 (Springer, Cham, 2017), p. 381.

[5] J.-M. Ginoux, From Nonlinear Oscillations to Chaos Theory, in *The Foundations of Chaos Revisited: From Poincaré to Recent Advancements, Understanding Complex Systems*, edited by C. H. Skiadas (Springer, Cham, 2016), pp. 27–47.

[6] E. Pugliese, R. Meucci, S. Euzzor, J. G. Freire, and J. A. C. Gallas, Complex dynamics of a dc glow discharge tube: Experimental modeling and stability diagrams, Sci. Rep. **5**, 8447 (2015).

[7] L. O. Chua, Memristor–The missing circuit element, IEEE Trans. Circuit Theory **18**, 507 (1971).

[8] L. O. Chua, Resistance switching memories are memristors, Appl. Phys. A **102**, 765 (2011).

[9] D. B. Strukhov, G. S. Snider, G. R. Stewart, and R. S. Williams, The missing memristor found, Nature (London) **453**, 80 (2008).

[10] J.-M. Ginoux, R. Meucci and S. Euzzor, A. Di Garbo, Torus breakdown in a uni junction memristor, Int. J. Bifurcation Chaos **28**, 1850128 (2018).

[11] G. Buzsaki, *Rhythms of the Brain* (Oxford University Press, New York, 2006), pp. 136–143.

[12] A. T. Winfree, *The Geometry of Biological Time* (Springer, New York, 1980), p. 779.

[13] J. Grasman and M. J. W. Jansen, Mutually synchronized relaxation oscillators as prototypes of oscillating systems in biology, J. Math. Biol. **7**, 171 (1979).

[14] I. R. Epstein and K. Showalter, Nonlinear chemical dynamics: Oscillations, patterns and chaos, J. Phys. Chem. **100**, 13132 (1996).

[15] S. Kumar, J. P. Strachan, and R. S. Williams, Chaotic dynamics in nanoscale NbO_2 Mott memristors for analogue computing, Nature (London) **548**, 318 (2017).

[16] Y. Hasewaga, R. Tanada, and Y. Ueda, On rational phase-locking oscillations of a simple sawtooth oscillator with UJT, Int. J. Bifurcation Chaos **11**, 3003 (2001).

[17] J. P. Keener, F. C. Hoppensteadt, J. Rinzel, Integrate-and-fire models of nerve membrane response to oscillatory input, SIAM J. Appl. Math. **41**, 503 (1981).

[18] A. Di Garbo, M. Barbi, and S. Chillemi, Dynamical behavior of the linearized version of the Fitzhugh–Nagumo neural model, Int. J. Bifurcation Chaos **11**, 2549 (2001).

[19] M. J. Chacron, A. Longtin, K. Pakdamanb, Chaotic firing in the sinusoidally forced leaky integrate-and-fire model with threshold fatigue, Physica D **192**, 138 (2004).

[20] Y. V. Pershin and M. Di Ventra, Current-voltage characteristics of semiconductor/ferromagnet junctions in the spin-blockade regime, Phys. Rev. B **77**, 073301 (2008).

[21] A. P. James, F. Shariff, and A. K. Maan, A neuron based switch: Application to low power mixed signal circuits, in *ACE 2010, 2010 International Conference on Advances in Computer Engineering, 20–21 June 2010, Banglaore* (IEEE, Piscataway, NJ, 2010), pp. 86–89.

[22] F. T. Arecchi, G. Giacomelli, A. Lapucci, and R. Meucci, Dynamics of a CO_2 laser with delayed feedback: The short-delay regime, Phys. Rev. A **43**, 4997 (1991)

[23] Y. Jeong, M. A. Zidan, and W. D. Lu, Parasitic effect analysis in memristor array-based neuromorphic systems, IEEE Trans. Nanotechnol. **17**, 184 (2018).

[24] A. Pikovsky, M. Rosenblum, and J. Kurths, *Synchronization* (Cambridge University Press, Cambridge, 2003), p. 432.

[25] T. Matsumoto, L. O. Chua, and R. Tokunaga, Chaos via torus breakdown, IEEE Trans. Circuits Syst. **34**, 240 (1987).

[26] M. S. Baptista and I. L. Caldas, Dynamics of the two-frequency torus breakdown in the driven double scroll circuit, Phys. Rev. E **58**, 4413 (1998).

[27] E. Ott, *Chaos in Dynamical Systems* (Cambridge University Press, Cambridge, 1993), p. 492.

[28] A. H. Nayfeh and B. Balachandran, *Applied Nonlinear Dynamics* (John Wiley & Sons, New York, 1995), p. 314.

[29] M. T. Rosenstein, J. J. Collins, and C. J. De Luca, A practical method for calculating the largest Lyapunov exponents from small data sets, Physica D **65**, 117 (1993).